Conformational Studies on the Selectin and Natural Killer Cell Receptor Ligands Sulfo- and Sialyl-lacto-*N*-fucopentaoses (SuLNFPII and SLNFPII) Using NMR Spectroscopy and Molecular Dynamics Simulations. Comparisons with the Nonacidic Parent Molecule LNFPII[†]

Heide Kogelberg,*[,‡] Thomas A. Frenkiel,[§] Steve W. Homans,[||] André Lubineau,[⊥] and Ten Feizi[‡]

The MRC Glycosciences Laboratory, Northwick Park Hospital, Watford Road, Harrow, Middlesex, HA1 3UJ, U.K., MRC Biomedical Nuclear Magnetic Resonance Centre, National Institute for Medical Research, The Ridgeway, Mill Hill, London NW7 1AA, U.K., Institute of Biomolecular Sciences, School of Chemistry, University of St. Andrews, St. Andrews, Fife KY16 9ST, Scotland, U.K., and Laboratoire de Chimie Organique Multifonctionnelle, Université de Paris−Sud, Bat. 420, 91405 Orsay Cedex, France

Received September 11, 1995; Revised Manuscript Received November 28, 1995[⊗]

ABSTRACT: This investigation is focused on the conformational behavior of the blood group Lewis[a] (Le[a])-active pentasaccharide lacto-*N*-fucopentaose II (LNFPII) and its sulfated and sialylated analogs, SuLNFPII and SLNFPII. The latter two are more potent oligosaccharide ligands for the animal lectins, E- and L-selectin, and the natural killer cell receptor, NKR-P1, than are the shorter chain analogs based on the trisaccharide Le[a] domain. We report here that the three oligosaccharides based on the fucopentasaccharide have very similar average solution conformations as determined from NMR spectroscopical parameters, in particular ^{13}C chemical shift differences. From restrained simulated annealing and restrained molecular dynamics (MD) simulations performed in order to determine the most probable conformational distributions around the glycosidic linkages we derive models for these oligosaccharides that are in good agreement with experimental parameters, such as rotating-frame Overhauser effects (ROE's) and long-range $^{1}H,^{13}C$ coupling constants across the glycosidic linkages. In these model structures the Le[a] domain at the nonreducing end of the longer chain oligosaccharides approximates the same rigid structure as in the shorter analogs. The Galβ1−4Glc linkage at the reducing end is also rather rigid, showing only little more flexibility than the Le[a] domain. However, the NeuAcα2−3Gal linkage in SLNFPII, and the GlcNAcβ1−3Gal linkage in all three oligosaccharides are flexible, in each case fluctuating mainly between two minimum energy structures: ($\phi = -81°$, $\psi = 8°$) and ($\phi = -160°$, $\psi = -20°$) for the NeuAcα2−3Gal linkage, as reported previously for the isomeric sequence 3′-sialyl Le[x], and ($\phi = -25°$, $\psi = -26°$) and ($\phi = 20°$, $\psi = 24°$) for the GlcNAcβ1−3Gal linkage. The flexibility of the latter linkage may allow the lactosyl domain at the reducing end to fit with little strain into extended carbohydrate binding sites on the recognition proteins, and, for the purposes of drug designs, it will be important to establish which conformational distribution is assumed for the GlcNAcβ1−3Gal linkage in these longer chain oligosaccharides in the bound state.

Oligosaccharides of the blood group family decorate diverse glycoproteins and glycolipids on the surface of cells. Work with monoclonal antibodies highlighted the remarkable changes that occur in the display of the individual oligosaccharide sequences during cellular differentiation and maturation (Feizi, 1981, 1985; Hakomori, 1985). These apparently programmed changes were regarded as possible clues to the roles of this family of oligosaccharides as "area codes" which determine cell migration pathways and as ligands in macromolecular interactions in health and disease (Feizi & Childs, 1987). These concepts have received much support from developments in vascular biology and inflammation research which resulted in the cloning and sequencing of proteins such as the selectins, which have important roles as cell adhesion molecules at the initial stages of leucocyte recruitment (Bevilacqua & Nelson, 1993), and the effector molecule, NKR-PI, on natural killer (NK) cells (Giorda et al., 1990) which has a crucial role (Bezouška et al., 1994) in recognition and killing of certain tumor cells and virally infected cells. These proteins are lectins that act through recognition of oligosaccharides (Bevilacqua & Nelson, 1993; Bezouška et al. 1994). Among the ligands for these effector proteins are acidic oligosaccharides based on the blood group-related trisaccharide antigens Le[a] and Le[x] (Figure 1), namely, their 3′-sialyl and 3′-sulfated forms (Feizi, 1993). With E- and L-selectin (Yuen et al., 1992, 1994) as well as NKR-P1 (Bezouška et al., 1994) the longer chain analogs of these oligosaccharides based on the pentasaccharides lacto-*N*-fucopentaose II (LNFPII)[1] and lacto-*N*-fucopentaose III (LNFP III) or on the tetrasaccharides lacto-*N*-fucotetraoses II and III have been shown to be more potent ligands than

[†] This work is supported by the Leukaemia Research Fund Project Grant 9348 and by the Medical Research Council Program Grant E400/622.

* Corresponding author: Tel: +44 (0)181 869 3465. FAX: +44 (0)181 869 3455.

[‡] The MRC Glycosciences Laboratory.

[§] MRC Biomedical Nuclear Magnetic Resonance Centre.

[||] University of St. Andrews.

[⊥] Université de Paris−Sud.

[⊗] Abstract published in *Advance ACS Abstracts,* January 15, 1996.

0006-2960/96/0435-1954$12.00/0

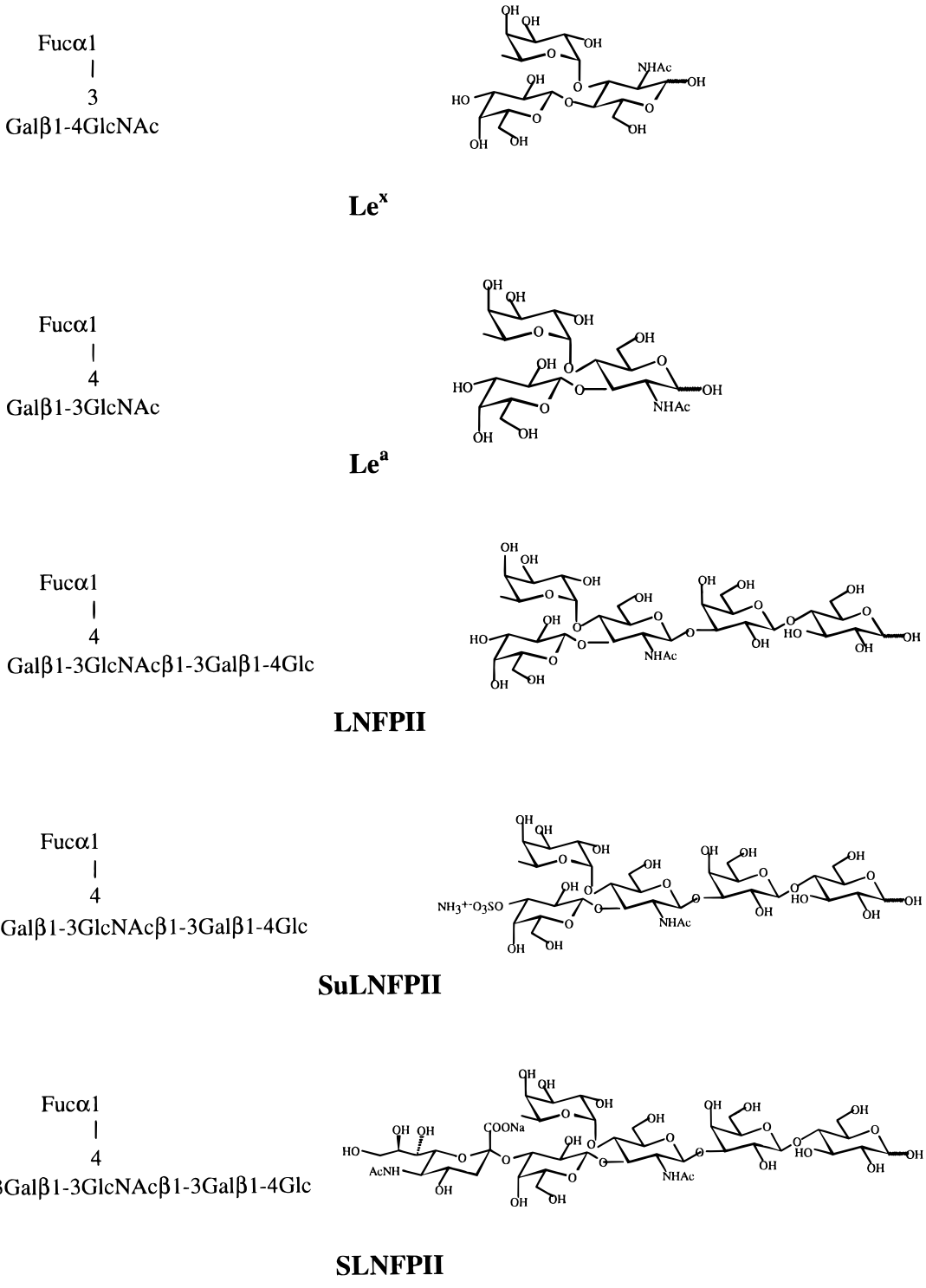

FIGURE 1: Structures of Le^x, Le^a, LNFPII, SuLNFPII, and SLNFPII.

the short chain analogs. In view of the optimism (Bezouška et al., 1994) that these blood group related oligosaccharides or their analogs may find a place in therapeutics for the inhibition or enhancement of immune effector functions, it is of special interest to understand their conformational behavior.

Conformational studies of di- and trisaccharides that constitute epitopes for blood group related antigens have shown that their three-dimensional structures are rather rigid. The glycosidic linkages of the blood group Le^a and Le^x determinants (for structures see Figure 1) occupy the same conformational space (Bush & Cagas, 1992, and references therein), and introduction of sialic acid (Bechtel et al., 1990; Ichikawa et al., 1992; Lin et al., 1992; Ball et al., 1992) or

[1] Abbreviations: COSY, correlated spectroscopy; Fuc, L-fucopyranose; Gal, D-galactopyranose; Glc, D-glucopyranose; GlcNAc, 2-acetamido-2-deoxy-D-glucopyranose; HMQC, heteronuclear multiple-quantum correlation; ISPA, independent spin-pair approximation; LNFPII, lacto-*N*-fucopentaose II, Lewis^a pentasaccharide; LNFPIII, lacto-*N*-fucopentaose III, Lewis^x pentasaccharide; MD, molecular dynamics; NeuAc, D-neuraminic acid; NOE, nuclear Overhauser effect; ROE, rotating-frame Overhauser effect; ROESY, rotating-frame Overhauser effect spectroscopy; SLe^a, sialylated Lewis^a tetrasaccharide; SLe^x, sialylated Lewis^x tetrasaccharide; SLNFPII, sialylated Lewis^a hexasaccharide; SuLe^a, sulfated Lewis^a trisaccharide; SuLNFPII, sulfated Lewis^a pentasaccharide; TOCSY, total correlation spectroscopy.

sulfate (Kogelberg & Rutherford, 1994) to the 3-position of galactose does not affect the average conformations of the Le^a and Le^x moieties. The NeuAcα2−3Gal linkage of SLe^x, however, has been shown to be flexible and to fluctuate mainly between two of the minimum energy structures (Mukhapadhyay et al., 1994; Rutherford et al., 1994).

In the present study we have investigated the conformational behavior of the superior selectin ligands with extended backbones: SuLNFPII and SLNFPII. Also included in this study is the parent molecule LNFPII. Complete ^1H and ^{13}C chemical shift assignments, prerequisites for the conformational studies, were derived from TOCSY, TOCSY−ROESY, HMQC, and 2D single-quantum multiple-bond correlation spectra. In order to obtain the most probable distributions around the glycosidic linkages for these oligosaccharides we have used restrained simulated annealing and restrained molecular dynamics (MD) simulations. Upper limits of distance restraints were obtained from 2D-ROESY spectra. For partially overlapping signals these restraints were derived from 1D-ROESY spectra. Special emphasis was on obtaining information on the conformational distributions for the GlcNAcβ1−3Gal and Galβ1−4Glc linkages in these oligosaccharides. In order to evaluate the theoretical models, back-calculated ROE's and long-range $^1H,^{13}C$ coupling constants across the glycosidic linkages ($^3J_{C,H}$) were compared with those parameters obtained experimentally. A 2D single-quantum multiple-bond correlation experiment and proton-detected selective 1D experiments were used to obtain the $^3J_{C,H}$ values, relying on the natural abundance of ^{13}C.

MATERIAL AND METHODS

NMR Spectroscopy. LNFPII [Galβ1−3(Fucα1−4)-GlcNAcβ1−3Galβ1−4Glc] was obtained from Dextra Laboratories, Reading, U.K. SuLNFPII [$NH_4^+SO_3^-$-3Galβ1−3(Fucα1−4)GlcNAcβ1−3Galβ1−4Glc] was synthezised chemically (Lubineau et al., 1995). SLNFPII [NeuAcα2−3Galβ1−3(Fucα1−4)GlcNAcβ1−3Galβ1−4Glc] was obtained from V. Piskarev, Institute of Food Substances, Moscow, Russia. All samples contained ^{13}C at natural abundance.

Spectra were recorded on Bruker AM-400 (400.13 MHz ^1H and 100.16 MHz ^{13}C), Bruker AM-500 (500.13 MHz ^1H and 125.8 MHz ^{13}C), Varian UNITY *plus*-500 (500.13 MHz ^1H and 125.8 MHz ^{13}C), and Varian UNITY-600 (599.92 MHz ^1H and 150.86 MHz ^{13}C). The samples were prepared by repeated disolution/lyophilization from D_2O. Finally, 5 mg of LNFPII and 1 mg or, for heteronuclear experiments, 6 mg of SLNFPII and 6 mg of SuLNFPII were dissolved in 0.6 mL of D_2O. All NMR data sets were recorded at 20 °C, except the 2D single-quantum multiple-bond correlation experiment for SuLNFPII, which was obtained at 27 °C. The observed ^1H chemical shifts were reported relative to internal acetone (2.225 ppm). The carbon chemical shifts were quoted relative to the methyl group of internal acetone (31.07 ppm). 1D-NMR spectra were typically recorded using 4000 Hz in the ^1H-NMR spectra and 25 000 Hz in the broad-band ^1H-decoupled ^{13}C-NMR spectra.

1D-TOCSY spectra (Kessler *et al*., 1989), of 64 scans each, were obtained using a Gaussian pulse of 93 or 60 ms, depending on desired selectivity. The duration of the spin−lock period, realized via the MLEV-17 sequence (Bax & Davies 1985b), was 140 ms. 1D-ROESY spectra (Kessler *et al*., 1989), of 64 scans each, were acquired in a manner similar to the 1D-TOCSY spectra using spin−lock mixing times of 300 ms. Different mixing times were applied initially in order to establish that the ROE's lie in the initial slope of the ROE buildup curve and hence allowing for the simple "two-spin approximation" or independent spin-pair approximation (ISPA) used in this study. H5 and H6 for Gal^3 and Gal^4 for SuLNFPII and SLNFPII were assigned using 1D-TOCSY−ROESY experiments in a manner similar to those described by Poppe and van Halbeek (1992).[2] The TOCSY selective pulse was a 93 ms Gaussian pulse, and the ROESY selective pulse was a 60 ms Gaussian pulse. Mixing times of 140 and 300 ms were used for the TOCSY transfer and for the ROESY step, respectively. For SuLNFPII 512 scans and for SLNFPII 4096 scans were acquired.

2D-COSY spectra were acquired in magnitude mode using acquisition times of 233 ms in t_1 and 0.6 s in t_2 with 16 scans in each t_1 increment. Data matrices of 800(t_1) × 4096(t_2) points were acquired, zero-filled to 2048(t_1) × 4096(t_2) points and multiplied prior to Fourier transformation by a sine bell function.

2D-ROESY (Bax & Davies, 1985a) spectra were acquired with a 300 ms spin−lock period. Acquisition times of 158 ms and 0.63 s were used in t_1 and t_2, respectively. Eight scans were acquired in each of 1024 experiments into 4096 data points. The 2D matrix was zero-filled to 2048(t_1) × 8192(t_2) data points and multiplied by a Gaussian function in both dimensions. Spectra were base line corrected before volume integration using VNMR software. Cross-peak volumes from both sides of the diagonal were averaged. The spectrum offset was set at the downfield edge of the spectrum in order to minimize TOCSY transfer. A cross-peak for a proton pair with unknown distance was normalized to a cross-peak for a known intra-pyranose proton pair (see Tables 1 and 2).

2D-HMQC spectra (Müller, 1979; Bax *et al*., 1983a,b; Bendall *et al*., 1983) for LNFPII and SLNFPII were acquired with 73 ms in t_1 and 0.15 s in t_2, together with 32 scans per t_1 increment. ^1H decoupling was employed using the GARPI sequence. The data matrix (t_1,t_2) consisted of 1024 × 768 points and was zero-filled to 2048 × 2048 points and multiplied by a Gaussian function prior to Fourier transformation. Spectra were recorded in pure phase-absorption mode by collecting hypercomplex data (States *et al*., 1982).

Three-bond proton−carbon coupling constants spanning the glycosidic linkages of SLNFPII were obtained by proton-detected 1D experiments based on those introduced by Poppe and van Halbeek (1991a,b). Two different methods were used. One, based on Poppe and van Halbeek (1991a), was used for long-range couplings involving H1 protons; it differed from that described by Poppe and van Halbeek (1991a) primarily in making use of pulsed field gradients to select magnetization which followed the desired pathway via ^{13}C at an intermediate stage of the sequence. In our experience this resulted in much improved suppression of the unwanted signals from protons that are not coupled to ^{13}C. A delay of 100 ms was allowed for evolution of the CH couplings and the selective ^{13}C and ^1H 180° pulses had lengths of 5 and 43 ms respectively. Four such double-

[2] A superscript at the name of a sugar residue indicates to which position of the adjacent monosaccharide it is glycosidically linked, e.g., Gal^3 means Galβ1−3GlcNAc and Gal^4 means Galβ1−4Glc.

Table 1: Experimental ROE's from 1D- and 2D-ROESY Experiments at 20 °C Using 300 ms Mixing Times, Average $^1H-^1H$ Distances Calculated from Those ROE's, Theoretical Average $^1H-^1H$ Distances Back-Calculated from 1 ns Molecular Dynamics Simulations, and Theoretical ROE's Calculated from Those Distances on Sulfated LNFPII (SuLNFPII)

	measured ROE (relative units)		average $^1H-^1H$ distances from experiment (Å)[a]				
proton pairs	1D	2D	1D	2D	constraints[b]	simulated ROE[a] (relative units)	simulated average $^1H-^1H$ distances (Å)[a]
FucH5−Gal^{3}H2	1.2	1.1	2.3[c]	2.3[c]	s	1.00[c]	2.35
FucH6−Gal^{3}H2	1.4	1.2	2.9[d]	3.0[d]	m[e]	2.50[d]	2.67
GlcNAcCH$_3$−Gal^{3}H1	det.[f]	det.[f]			w[e]		3.46
Gal^{3}H1−GlcNAcH3	1.1	1.1	2.5[g]	2.5[g]	s	1.27[g]	2.46
GlcNAcH1−Gal^{4}H3	1.2	1.4	2.3[h]	2.3[h]	s	1.43[h]	2.27
FucH1−GlcNAcH4	0.9	det.[i]	2.5[j]		s	0.95[j]	2.48
FucH1−GlcNAcH6$_R$	0.6	det.[i]	2.7[j]		m	1.66[j]	2.26
Gal^{4}H1−GlcH4	0.9	det.[k]	2.2[l]		s	0.60[l]	2.32
Gal^{4}H1−GlcH6a,6b	0.3	det.[k]	2.6[l]		m[e]	0.28, 0.24[l]	2.64, 2.71

[a] See Materials and Methods for how these values were derived. [b] ROE restraints are classified as strong (s, 1.8−2.7 Å), medium (m, 1.8−3.3 Å), and weak (w, 1.8−5.0 Å). [c] Reference ROE FucH5−FucH3, reference distance = 2.35 Å. [d] Reference ROE FucH6−FucH4, mean reference distance = 3.11 Å. [e] These distances were defined as arithmetic averages of the coordinates of the methyl- or methylene protons. [f] Detectable, but no reference distance available. [g] Reference ROE Gal^{3}H1−Gal^{3}H3, reference distance = 2.56 Å. [h] Reference ROE GlcNAcH1−GlcNAcH5, reference distance = 2.41 Å. [i] Detectable, however GlcNAcH4 and FucH2 are strongly overlapping and cannot be integrated separately. [j] Reference ROE FucH1−FucH2, reference distance = 2.46 Å. [k] Detectable, however Gal^{4}H2 and GlcH4 are strongly overlapping and cannot be integrated separately. [l] Reference ROE Gal^{4}H1−Gal^{4}H3 + Gal^{4}H1−Gal^{4}H5, reference distances = 2.56 + 2.28 Å.

Table 2: Experimental ROE's from 1D- and 2D-ROESY Experiments at 20 °C Using 300 ms Mixing Times, Average $^1H-^1H$ Distances Calculated from those ROE's, Theoretical Average $^1H-^1H$ Distances Back-Calculated from 1 ns Molecular Dynamics Simulations, and Theoretical ROE's Calculated from Those Distances on Sialylated LNFPII (SLNFPII)

	measured ROE (relative units)		$^1H-^1H$ distance from experiment (Å)[a]				
proton pair	1D	2D	1D	2D	constraints[b]	simulated ROE[a] (relative units)	simulated $^1H-^1H$ distance (Å)[a]
FucH5−Gal^{3}H2	1.3	1.1	2.3[c]	2.3[c]	s	0.98[c]	2.36
FucH6−Gal^{3}H2	1.5	1.2	2.9[d]	3.0[d]	m[e]	2.55[d]	2.66
Gal^{3}H1−GlcNAcH3	1.0	det.[f]	2.6[g]		s	1.24[g]	2.47
GlcNAcH1−Gal^{4}H3	1.4	1.3	2.3[h]	2.3[h]	s	1.36[h]	2.29
FucH1−GlcNAcH4	0.9	det.[i]	2.5[j]		s	1.00[j]	2.46
FucH1−GlcNAcH6$_R$	0.5	det.[i]	2.8[j]		m	1.64[j]	2.22
Gal^{4}H1−GlcH4	0.7	0.8	2.3[k]	2.2[k]	s	0.57[k]	2.34
Gal^{4}H1−GlcH6a,6b	0.3	0.2	2.7[k]	2.8[k]	m[e]	0.28, 0.27[k]	2.64, 2.65
NeuAcH3$_{ax}$−Gal^{3}H3	0.3	0.4	3.2[l]	3.0[l]	w	0.73[l]	2.79
NeuAcH8−Gal^{3}H3		0.2		3.4[g,m]	w	0.21[m]	3.43
GlcNAc(*Ac*)−Gal^{3}H1		det.			w[e]		3.44

[a] See Materials and Methods for how these values were derived. [b] ROE restraints are classified as strong (s, 1.8−2.7 Å), medium (m, 1.8−3.3 Å), and weak (w, 1.8−5.0 Å). [c] Reference ROE FucH5−FucH3, reference distance = 2.35 Å. [d] Reference ROE FucH6−FucH4, mean reference distance = 3.11 Å. [e] These distances were defined as arithmetic averages of the coordinates of the methyl- or methylene protons. [f] Detectable, however Gal^{3}H3 and GlcNAcH3 are strongly overlapping and cannot be integrated seperately. [g] Reference ROE Gal^{3}H1−Gal^{3}H3, reference distance = 2.56 Å. [h] Reference ROE GlcNAcH1−GlcNAcH5, reference distance = 2.41 Å. [i] Detectable, however FucH2 and GlcNAcH4 are partially overlapping and cannot be integrated seperately. [j] Reference ROE FucH1−FucH2, reference distance = 2.46 Å. [k] Reference ROE Gal^{4}H1−Gal^{4}H3 + Gal^{4}H1−Gal^{4}H5, reference distance = 2.56 + 2.28 Å. [l] Reference ROE NeuAcH3ax−NeuAcH5, reference distance = 2.65 Å. [m] The contribution from GlcNAcH3, which also gives an ROE with Gal^{3}H1, has been subtracted.

selective experiments were carried out: 6400 transients were acquired for each experiment, resulting in a total recording time of 18 h. The acquisition time in each experiment was 1 s, and the data were zero-filled to give a final digital resolution of 0.122 Hz/point.

A second method was used to measure the three-bond coupling between NeuAcC2 and Gal^{3}H3. This was based on Poppe and van Halbeek (1991b) but contained a selective 180° ^{13}C pulse (of length 5 ms) in place of the ^{13}C chemical-shift filter employed by Poppe and van Halbeek. Pulsed field gradients were also used for pathway selection, as described above. A total of 16880 scans were averaged, with an acquisition time of 2 s. The data were zero-filled to give a final digital resolution of 0.122 Hz/point. This experiment took 14 h to record.

A 2D single-quantum multiple-bond correlation experiment (Norwood *et al*., 1990) was used to obtain long-range proton−carbon coupling constants for SuLNFPII. This was recorded on a Bruker AM-500 spectrometer, using acquisition times of 51.2 ms in t_1 and 1.4 s in t_2. A total of 512 increments were acquired, with 192 scans per increment. The data matrix was multiplied prior to Fourier transformation by a exponential function and zero-filled once in the t_1 and t_2 dimensions to give a final digital resolution of 9.8 Hz/point in F1 and 0.2 Hz/point in F2. The data took 58 h to acquire.

Computational Methods. All calculations were performed with the molecular modeling package DISCOVER version 2.96 (Biosym Technologies Inc.) interfaced to the AMBER force field using the force field parameters derived for oligosaccharides (Homans, 1990) but without torsional terms desribing the *exo*-anomeric potentials. Parameters describing the sulfate group were as reported previously (Kogelberg & Rutherford, 1994). The calculations were run *in vacuo* on a Silicon Graphics Personal Iris Workstation, and the dielectric constant was set to 80. For all graphical depictions the software package INSIGHT version 2.3.5 (Biosym Technologies Inc.) was used.

Dihedral angles ϕ and ψ at the glycosidic linkages were defined as follows: ϕ = H1−C1−O1−C*x*, ψ = C1−O1−C*x*−H*x*, with *x* being the aglyconic linkage site. The NeuAcα2−3Gal linkage was defined as ϕ = C1−C2−O3−C3 and ψ = C2−C3−O3−H3.

The three-dimensional starting structures for SuLNFPII and SLNFPII were chosen to be of relative low energy. The conformation around the Galβ1−3GlcNAc and Fucα1−3GlcNAc linkages was taken from Kogelberg and Rutherford (1994). Then one monosaccharide unit was added at a time, and a two-parameter ϕ,ψ map was obtained by generating a grid of energy values at 5° increments over the entire range of possible ϕ and ψ combinations. First Gal was added to GlcNAc, and then Glc was added to Gal[4]. For SLNFPII finally NeuAc is linked to the 3-position of Gal[3]. At each grid the molecule was optimized except for the ϕ and ψ dihedrals of the GlcNAcβ1−3Gal, Galβ1−4Glc, or NeuAcα2−3Gal linkages. These were constrained to their target values by adding a strong harmonic potential (50 000 kcal/rad^2) to their torsional potential.

From these low-energy structures 10 random structures were generated by performing short MD runs at 750 K for 10 ps with time intervals of 1 fs. These structures were optimized by restrained simulated annealing, running 1 ps of MD at each temperature step from 500 to 300 K (in 50 K steps), then 10 K (with 10 K steps) and finally at 5 K. The lowest energy geometries were used as input to 1 ns dynamics simulations. In an initial equilibrium step, the system was coupled to a thermal bath at 300 K and was pre-equilibrated for 10 ps with a time step of 1 fs. The dynamics runs were then continued for 1 ns with a time step of 1 fs. ROE constraints were included as a biharmonic potential function, with a force constant of 10 kcal/mol/Å^2 and a maximum force of 10 kcal/mol/Å. Coordinates for protons of methyl- and methylene groups were defined as arithmetic averages. Time-averaged ^{1}H−^{1}H distances ($<r^{-6}>^{-1/6}$) and time-averaged $^3J_{C,H}$ values were extracted using the md-process program each 250 steps after the system had equilibrated. The average $^3J_{C,H}$ values were calculated from Karplus-type curves (Mulloy *et al*., 1989). Experimental ^{1}H−^{1}H distances were calculated from the experimentally obtained ROE values and a reference distance (assuming a simple r^{-6} dependence of the ROE values). Theoretical relative ROE values were calculated from the ratio of the average ^{1}H−^{1}H distances and a reference distance (assuming a simple r^{-6} dependence of the ROE values).

RESULTS

NMR Experiments

^{1}H and ^{13}C Chemical Shift Assignments. ^{13}C chemical shift assignments for the parent molecule, LNFPII, were derived from a HMQC spectrum using the reported ^{1}H chemical shifts (Cagas & Bush, 1990). Complete ^{1}H and ^{13}C chemical shift assignments for SuLNFPII and SLNFPII were derived from 1D-TOCSY, 1D-TOCSY−ROESY, 2D-HMQC, and 2D single-quantum multiple-bond correlation spectra. Assignments for the reporter group protons for SuLNFPII were reported in the original paper describing the synthesis (Lubineau, et al., 1996). Previously reported ^{1}H chemical shifts for LNFPII (Cagas & Bush, 1990), Le^a (Bechtel et al., 1990), and SLe^a (Bechtel et al., 1990), and both ^{1}H and ^{13}C chemical shifts for SuLe^a (Kogelberg & Rutherford, 1994) and SLe^x (Ichikawa et al., 1992) helped in making the assignments.

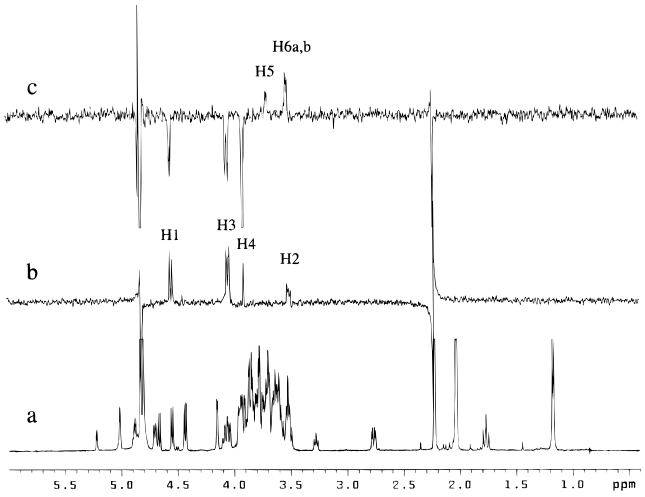

FIGURE 2: ^{1}H-NMR spectra of an α,β anomeric mixture of SLNFPII. (a) One-dimensional ^{1}H-NMR reference spectrum, (b) one-dimensional TOCSY spectrum with selective irradiation of Gal^{3}H1 (140 ms mixing time), and (c) one-dimensional TOCSY−ROESY spectrum with double-selective irradiation of Gal^{3}H1 and Gal^{3}H4 in succession. Isotropic mixing time was the same as in b, and the ROESY mixing time was 300 ms.

Selective 1D-TOCSY experiments were sufficient to derive at complete assignments for all protons for the GlcNAc and Glc residues in SuLNFPII and SLNFPII. Also Fuc can be assigned completely using this experiment because here FucH1 and additionally the downfield-shifted FucH5 can be excited selectively. However, by these means it is not possible to assign the H5, H6a, and H6b protons for the two Gal residues. Because of the small coupling constant between H4 and H5 (∼1 Hz), magnetization is only transferred up to H4 in the TOCSY step (illustrated in Figure 2b for the Gal^3 residue in SLNFPII). The assignment problem can be overcome by performing 1D-TOCSY−ROESY experiments. Figure 2c shows this technique applied to SLNFPII, first exciting Gal^3 H1, which results in the characteristic in-phase appearance for H3 and H4 from the TOCSY transfer, and second exciting Gal^{3}H4, which gives the "anti-phase" pattern for H5, H6a, and H6b as a result of the ROESY step.

^{1}H and ^{13}C Chemical Shift Differences. The effects of sulfation and sialylation on the average solution conformation of SuLNFPII and SLNFPII were addressed by comparing their chemical shifts with those for the parent molecule, LNFPII (Figure 3). Sulfation at the 3-position of Gal^3 results in the expected (Kogelberg & Rutherford, 1994) downfield ^{1}H chemical shift displacements of 0.677 ppm for H3, 0.422 ppm for H4, 0.143 ppm for H2, and 0.129 ppm for H1 (Figure 3a). The only carbon atoms noticeably affected by introduction of the sulfate group are C3, for which the shift displacement is 7.76 ppm to lower field, and the adjacent carbons C2 and C4, for which the displacement is 1.92 and 1.82 ppm, respectively, to higher field (Figure 3b). This is in accord with previous findings with SuLe^a (Kogelberg & Rutherford, 1994). Introduction of sialic acid at the 3-position of Gal^3 results in the expected (Bechtel et al, 1990; Ichikawa et al., 1992) downfield shift displacement of 0.421 ppm for H3 (Figure 3a) and 3.34 ppm for C3 and the high-

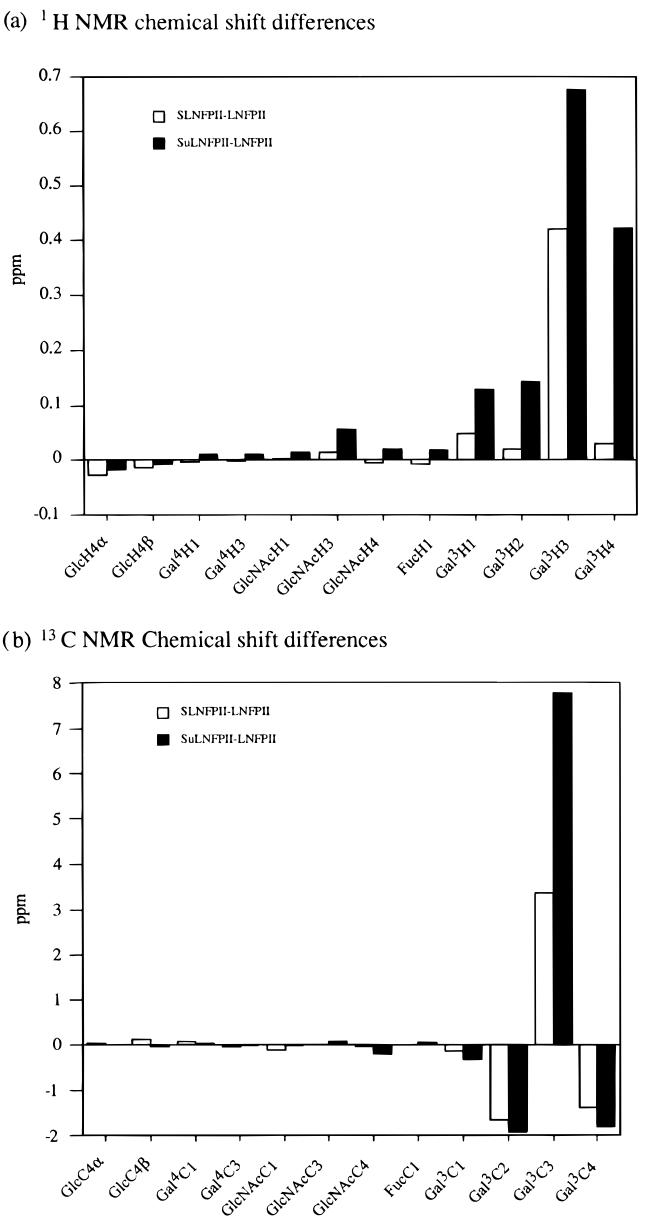

FIGURE 3: Differences (in ppm) of (a) ^{1}H chemical shifts and (b) ^{13}C chemical shifts of SuLNFPII and SLNFPII relative to the non-sulfated parent molecule LNFPII. The changes of the chemical shifts of Gal^{3}H1, Gal^{3}H2, Gal^{3}H3, Gal^{3}H4 and Gal^{3}C1, Gal^{3}C2, Gal^{3}C3, and Gal^{3}C4 indicate the direct effects from the sulfate or sialic acid groups. Proton and carbon atoms involved in glycosidic linkages are not affected by introduction of the acidic groups.

field shift displacement of 1.66 ppm for C2 and 1.38 ppm for C4 (Figure 3b).

As reported by Bock et al. (1986), ^{13}C chemical shift changes for carbon atoms near the glycosidic linkage can be correlated with possible changes in the conformation around the glycosidic linkage. The fact that the only chemical shift changes observed are those due to the direct influence of the sulfate or sialic acid groups indicates therefore strongly that SuLNFPII, SLNFPII, and LNFPII have very similar conformations in solution.

Measurement of ROE's. With the complete ^{1}H and ^{13}C chemical shift assignments in hand for SuLNFPII, LNFPII, and SLNFPII, we could proceed to investigate the conformational behavior of these oligosaccharides. Proton nuclear Overhauser effects (NOE's) and ROE's can be used to obtain information on the average geometry in solution. A NOESY spectrum at 500 MHz for SuLNFPII using a mixing time of 500 ms gave only very weak NOE's (data not shown), indicating a condition where the correlation time of the molecule approaches the inverse of the Lamor frequency. Therefore we used ROE's from selective 1D- and 2D-ROESY experiments in order to derive approximate average ^{1}H$-^1$H distances (Tables 1 and 2). Application of the selective 1D-ROESY experiments was particularly important for obtaining ^{1}H$-^1$H distances across the Fucα1$-$4GlcNAc linkage for SuLNFPII and SLNFPII, because GlcNAcH4 and FucH2 are partially overlapping, and across the Galβ1$-$4Glc linkage where Gal^{4}H2 and GlcH4 are partially overlapping in SuLNFPII. The higher digital resolution in the 1D experiment, if compared with the 2D analog, allows for extracting the individual contributions for these protons. However ROE's between protons in crowded regions of the spectrum can be obtained only from the 2D-ROESY spectra. The experimentally obtained ROE's for SuLNFPII and those for SLNFPII are very similar, supporting further the notion that these two molecules have very similar average conformations in solution.

There were two conclusions at this stage: (a) because the protons across the glycosidic linkages show strong ROE's in these oligosaccharides, they have on average syn-periplanar arrangements, and (b) because there are strong remote ROE's between FucH5$-$Gal^{3}H2 and FucH6$-$Gal^{3}H2, the Gal^3 and Fuc rings are in juxtaposition.

Additional ROE's were of further help to constrain the glycosidic linkages: those between the Gal^{3}H1 and the methyl group of GlcNAc, between FucH1 and the high-field-shifted proton H6b of GlcNAc [which was assumed to be H6$_R$ in anology with findings in literature for *gluco* configurated compounds (Bock & Duus, 1994)], between Gal^4-H1 and both H6 protons of Glc; in the case of SLNFPII there were additional ROE's between NeuAcH3ax and Gal^3-H3 and between NeuAcH8 and Gal^{3}H3, which was, however, only barely above the noise level at the 300 ms mixing time used in this study.

The ROE observed between the methyl group of GlcNAc and Gal^{3}H1 was used to unambiguously assign this methyl group. In addition the assignment of the methyl group of NeuAc could be made from an ROE between this methyl group and H7 of NeuAc.

The distances thus obtained were implemented as upper limit constraints in restrained MD simulations (see later).

Measurement of Long-Range ^{1}H,^{13}C Coupling Constants. For a glycosidic linkage with the general form H1$-$C1$-$O*x*$-$C*x*$-$H*x*, the dihedral angle ϕ depends on the three-bond coupling between H1 and C*x* while ψ depends on the coupling between C1 and H*x*.

For SuLNFPII both types of coupling constants were derived from the splitting in the F2 dimension of a 2D single-quantum multiple-bond experiment. In the case of SLNFPII, selective 1D proton-detected experiments were used to obtain three-bond couplings between H1 and C*x* (Figure 4), and a related experiment was used to derive the coupling between NeuAcC2 and Gal^{3}H3 (Figure 5). Further details of these experiments can be found above (see Materials and Methods). The multiplet patterns produced by all of these experiments contain in-phase components resulting from homonuclear couplings and anti-phase components from the desired heteronuclear couplings. The separations between the maxima and minima of the anti-phase components are

Table 3: Glycosidic Torsion Angles (deg) and Final Energies (in kcal/mol) after Restrained Simulated Annealing (SA) for Sulfated LNFPII (SuLNFPII) and Sialylated LNFPII (SLNFPII)

molecule	structure	ϕ/ψ NeuAcα2−3Gal	Galβ1−3GlcNAc	Fucα1−4GlcNAc	GlcNAcβ1−3Gal	Galβ1−4Glc	relative final energy
SuLNFPII	1		44.9/16.8	39.4/19.7	−22.5/−25.3	35.8/5.3	11.9
	2		49.9/9.0	42.1/22.4	−22.3/−25.5	36.4/0.6	13.6
	3		48.8/10.7	46.8/20.3	−23.7/−26.3	36.4/1.9	3.1
	4		45.8/8.4	44.6/23.0	−23.8/−25.9	37.4/2.9	0.4
	5		49.4/10.5	41.9/21.8	−22.1/−21.6	35.9/5.1	2.0
	6		49.6/10.7	41.7/21.7	−23.2/−23.1	36.3/1.4	2.7
	7		50.8/10.5	41.6/21.7	16.1/24.7	39.0/−1.1	0.0
	8		49.2/8.8	41.9/22.2	−24.2/−26.0	36.0/6.2	3.9
	9		48.5/9.7	42.3/22.5	21.6/23.8	37.6/−0.3	3.2
SLNFPII	1	−81.0/7.7	37.6/12.9	48.3/20.5	20.0/23.5	22.4/−7.8	5.3
	2	−85.4/16.3	51.1/10.7	42.4/22.7	−23.8/−23.0	48.0/1.6	0.0
	3	−79.4/6.6	47.5/15.6	38.6/19.5	−26.5/−25.3	48.3/1.8	1.5
	4	−160.6/−12.0	43.6/17.7	41.5/24.7	−24.7/−25.7	35.8/5.4	11.6
	5	−89.4/10.9	44.5/12.4	48.8/19.5	−27.0/−18.4	33.3/7.9	19.3
	6	−83.8/11.3	47.4/11.9	43.2/21.4	−24.4/−20.7	46.5/0.6	0.7
	7	−160.7/−16.2	48.2/11.2	42.9/22.1	−22.4/−21.7	23.4/−8.1	2.2
	8	−159.1/−15.3	43.9/17.9	38.2/19.6	−24.4/−25.1	36.1/5.2	2.8
	9	−155.6/−22.7	49.0/10.4	45.5/26.3	−22.4/−21.2	22.7/−7.8	4.0
	10	−158.4/−16.4	47.2/10.5	43.3/22.1	−25.7/−22.6	23.1/−8.2	5.6

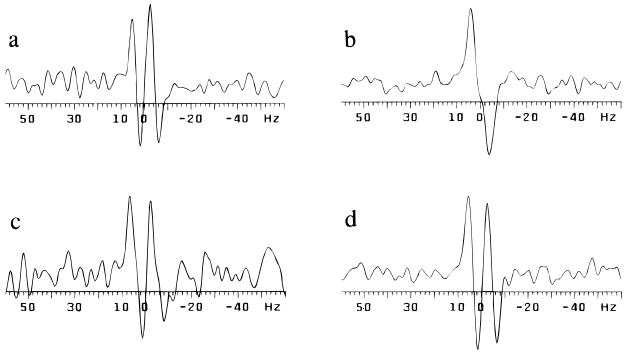

FIGURE 4: ^{1}H-NMR spectra of an α,β anomeric mixture of SLNFPII applying double-selective 180° ^{1}H and ^{13}C pulses in succession. The selective pulses were applied to (a) Gal^{3}H1 and GlcNAcC3, (b) FucH1 and GlcNAcC4, (c) GlcNAcH1 and Gal^{4}C3, and (d) Gal^{4}H1 and GlcC4.

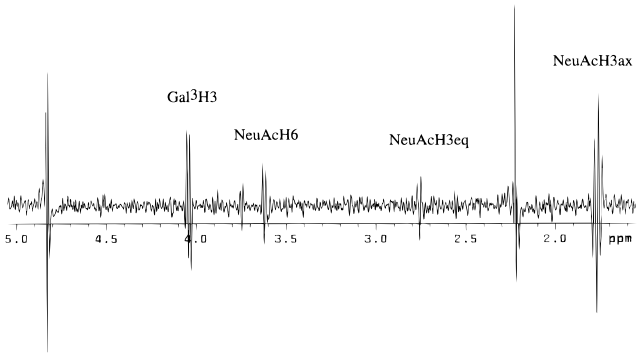

FIGURE 5: ^{1}H-NMR spectra of an α,β anomeric mixture of SLNFPII applying a selective 180° ^{13}C pulse to NeuAcC2.

reported in Table 4. However, because the line widths of the resonances are comparable to the coupling constants, these anti-phase splittings must be interpreted as upper limits for the heteronuclear coupling constants (Neuhaus *et al.* 1985).

In the case of the FucH1−GlcNAcC4 multiplet (Figure 4b), the homo- and heteronuclear couplings are very similar, and the inner lines of the multiplet cancel due to overlap of the anti-phase components. The value for the coupling constant between Gal^{3}H1 and GlcNAcC3 for SLNFPII in Table 4 has to be taken with additional caution as Gal^{3}C3, Gal^{3}C5, and GlcNAcC3 have very similar chemical shifts. Gal^{3}C3 and Gal^{3}C5 are expected to also give a coupling with Gal^{3}H1 of approximately 1.8 Hz (Mulloy et al., 1988). The observed anti-phase pattern will thus also contain contributions from these couplings, tending to reduce the apparent size of the Gal^{3}H1 and GlcNAcC3 coupling.

The splittings due to the three-bond H1-C*x* couplings are very similar for the Galβ1−3GlcNAc, Fucα1−4GlcNAc, and Galβ1−4Glc linkages, indicating similar average ϕ dihedral angles for these linkages. However, for the GlcNAcβ1−3Gal linkage the corresponding splitting is considerably larger (5.4 Hz), suggesting that the average dihedral angle ϕ for this linkage might be smaller than those for the other linkages. The anti-phase splittings for C1−H*x* couplings are all very similar, suggesting that the average dihedral angles ψ might be similar for all linkages.

$^3J_{C,H}$ values across the glycosidic linkages can be used to obtain average values for the dihedral angles ϕ and ψ by implementing an appropriate Karplus-type equation (Mulloy et al., 1988). Besides the ROE's these coupling constants are of importance in evaluating the theoretical models as they were not implemented as constraints in the simulations.

MOLECULAR MODELING CALCULATIONS

Restrained Simulated Annealed Structures. Reasonable low-energy starting structures for SuLNFPII and SLNFPII were derived by taking the published minimum energy structure (Kogelberg & Rutherford, 1994) for SuLe^a, adding sequentially the other monosaccharide units, and performing grid searches for each newly introduced glycosidic linkage. To gain information on the minimum energy structures which are assumed by these oligosaccharides in the presence of the experimentally derived constraints (Tables 1 and 2) we adopted a well-established protocol (Homans & Forster, 1992): generating 10 "random" structures from short MD runs at higher temperatures, which were subsequently annealed (Table 3). Both oligosaccharides anneal to very similar minimum energy structures in perfect agreement with the experimental data obtained from (a) the ^{13}C chemical shift displacements, (b) comparison of ROE's, and (c) long-

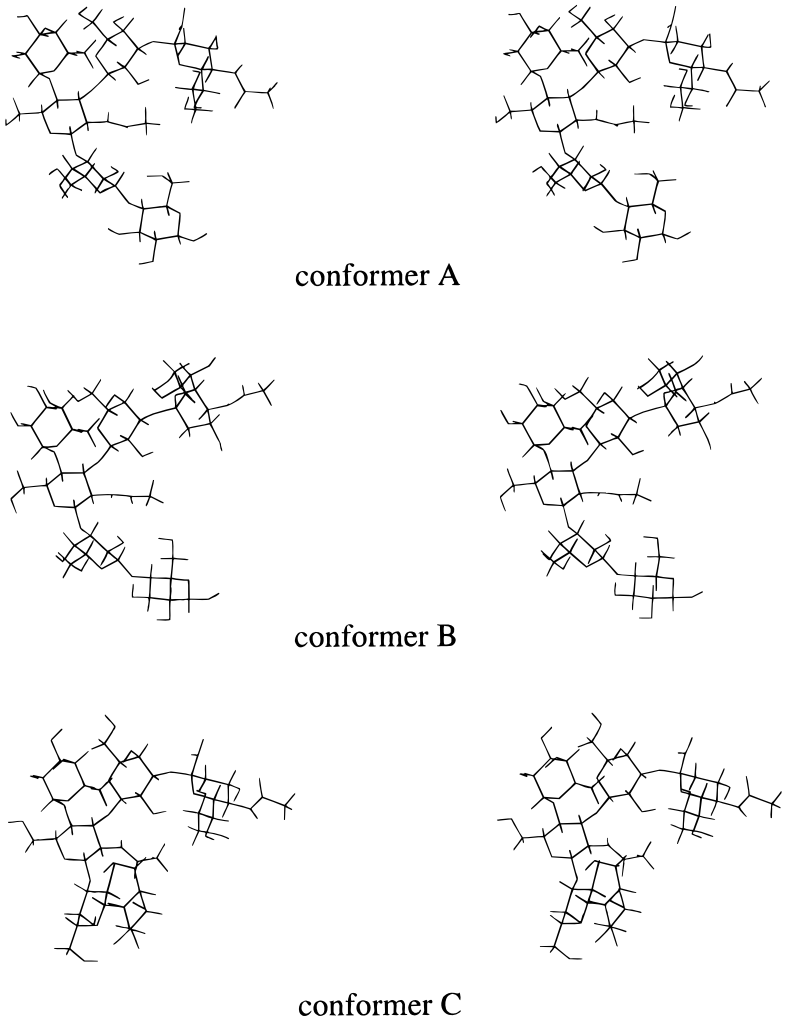

FIGURE 6: Stereoview of three minimum energy conformations of SLNFPII. The Glc at the reducing end is shown as the β-anomer. The Fuc-GlcNAc-Gal cores are virtually identical in the structures, but the ϕ and ψ dihedral angles for the NeuAcα2−3Gal linkage are −160.7/−16.2 (conformer B) and −79.4/6.6 and −81.0/7.7 (conformers A and C), those for the GlcNAcβ1−3Gal linkage were −26.5/−25.3 and −22.4/−21.7 (conformers A and B) and 20.0/23.5 (conformer C). For conformer B, NeuAcH3ax and Gal^{3}H3 across the NeuAcα2−3Gal linkage are in close proximity (2.3 Å), while in conformers A and C NeuAcH8 and Gal^{3}H3 are close (3.0 Å).

range ^{1}H,^{13}C coupling constants, as described. The Galβ1−3GlcNAc, Fucα1−4GlcNAc and Galβ1−4Glc linkages each fall within a very narrow range of conformational space. The NeuAcα2−3Gal linkage anneals to two different conformations (Figure 6), −79.4/6.6 and −81.0/7.7 (conformers A and C) and −160.7/−16.2 (conformer B), which are readily distinguishable, conformers A and C having a close proximity of NeuAcH8 to Gal^{3}H3 (3.0 Å) and conformer B having a close proximity of NeuAcH3ax to Gal^{3}H3 (2.3 Å). The glycerol side chain in NeuAc has the *trans* arrangement around the C7−C8 bond in all conformers. This arrangement has been shown previously (Breg et al., 1989) to be the sole conformer for the glycerol side chain in NeuAcα2−3Gal containing oligosaccharides. For the shorter chain SLe^a, using hard-sphere *exo*-anomeric effect calculations, the same two conformations around the NeuAcα2−3Gal linkage as found here were also reported to be those with the lowest energies (Bechtel et al., 1990). The same minimum energy structures for this linkage were obtained (Rutherford et al., 1994; Mukhapadhyay et al., 1994) by MD simulations for the isomeric molecule, SLe^x.

For the GlcNAcβ1−3Gal linkage nine of the 10 starting structures anneal to the same stable conformation −26.5/−25.3 and −22.4/−21.7 (conformers A and B), while the remaining structure anneals to an alternative conformation 20.0/23.5 (conformer C) (Figure 6) in SLNFPII. For SuLNFPII this alternative conformation was assumed twice. The conformation having ϕ,ψ dihedral angles for the NeuAcα2−3Gal linkage of around −160/−12 and for the GlcNAcβ1−3Gal linkage of around 20/24 was not seen by simulated annealing, but it could, of course, be expected to exist also.

Thus restrained simulated annealing established two possible sites of flexibility in the longer chain oligosaccharides: the terminal NeuAc residue and the Gal−Glc domain at the reducing end (Figure 7).

Restrained Molecular Dynamics Simulations. We then investigated the flexibility for all dihedral angles across the glycosidic linkages for SuLNFPII and SLNFPII using restrained MD simulations for 1 ns at 300 K, implementing the experimental ROE's as constraints. Theoretically back-calculated ^{1}H−^{1}H distances and long-range ^{1}H,^{13}C coupling constants across the glycosidic linkages could thus be compared with those from experiment (Tables 1, 2, and 4). Considering the qualitative approach undertaken in this study, there was very good agreement between experimental and theoretical ROE values. The back-calculated long-range ^{1}H,^{13}C coupling constants across the glycosidic linkages are

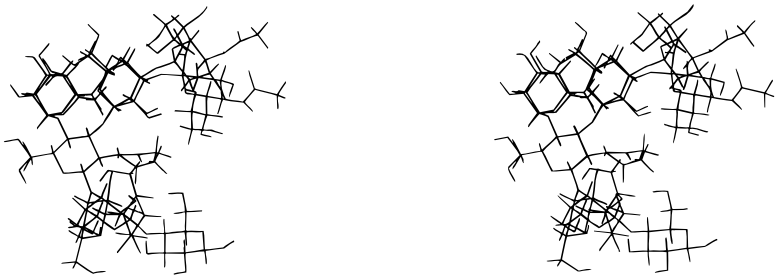

FIGURE 7: Conformers B and C (Figure 6) were superimposed onto GlcNAc, using the ring atoms and C6 for alignment, thus highlighting the different arrangement for the terminal NeuAc residues at the non-reducing end and for the Gal-Glc domains at the reducing end.

Table 4: Time-Averaged Glycosidic Torsion Angles (deg) from 1 ns Molecular Dynamics (MD) Simulations for Sulfated LNFPII (SuLNFPII) and Sialylated LNFPII (SLNFPII), with Root Mean Square (RMS) Deviations in Parenthesis and Average Long-Range ^{1}H,^{13}C Coupling Constants Back-Calculated from the MD Simulations ($^3J_{C,H}$, th)[a]

	ϕ/ψ				
molecule	NeuAcα2−3Gal	Galβ1−3GlcNAc	Fucα1-4GlcNAc	GlcNAcβ1−3Gal	Galβ1−4Glc
SuLNFPII					
dihedral ϕ,ψ, th		48.5 (12)/14.3 (10)	45.0 (11)/20.0 (9)	17.0 (24)/−16.6 (29)	42.2 (17)/2.9 (14)
$^3J_{C,H}$, th		2.6/5.1	2.9/4.8	5.0/5.0	3.1/5.4
$^3J_{C,H}$, exp[b]		≤3.1/≤5.1	≤3.8[c]/≤4.6	[d]/−	≤3.8/≤5.2
SLNFPII					
dihedral ϕ,ψ, th	-107.4 (43)/−4.4 (24)	49.4 (12)/15.1 (11)	43.4 (12)/20.6 (9)	13.3 (27)/−17.8 (30)	43.7 (16)/6.3 (12)
$^3J_{C,H}$, th	-/5.4	2.5/5.1	3.0/4.8	5.1/4.9	3.0/5.3
$^3J_{C,H}$, exp[e]	-/≤4.8	≤3.3[f]/−	≤4.0[c]/−	≤5.4/−	≤3.8/−

[a] Experimental long-range C,H coupling contants ($^3J_{C,H}$, exp) for SuLNFPII were obtained from a 2D single-quantum multiple-bond correlation experiment. Those for SLNFPII were derived from ^{1}H selective and ^{1}H,^{13}C double-selective proton-detected 1D experiments. The $^3J_{C,H}$, exp values represent upper limits of the real coupling constants (see text). [b] Error limits = ±0.8 Hz. [c] This coupling constant is extracted from the outer lines only. FucH1,H2 and FucH1,GlcNAcC4 have very similar coupling constants, hence the middle lines are canceled due to the anti-phase pattern. [d] GlcNAcH1 and H_2O have the same chemical shift at the chosen temperature. [e] Error limits = ±0.4 Hz. [f] GlcNAcC3 cannot be exited selectively, as Gal^{3}C3 and Gal^{3}C5 have very similar chemical shifts; this value is therefore likely to be an underestimate (see text).

also in reasonable good agreement with those obtained experimentally (Table 4). In particular, the larger $^3J_{H1,Cx}$ value between GlcNAcH1 and Gal^{4}C3, if compared with the $^3J_{H1,Cx}$ values for the other H1−C1−O*x*−C*x* linkages, is obtained experimentally and from the MD simulations. Trajectories for the evolution with time for all ϕ and ψ dihedral angles are shown for SLNFPII in Figure 8 a−j. Those for SuLNFPII were very similar (data not shown). The NeuAcα2−3Gal linkage in SLNFPII fluctuates between two low-energy states with approximate contributions of 65% for conformer A/C and 35% for conformer B (Figure 6). These average distributions are in agreement with experiment, showing a closer proximity for NeuAcH3ax to Gal^3-H3 than for NeuAcH8 to Gal^{3}H3; the latter, as would be expected, was only barely above the noise level. A similar distribution has been reported recently (Rutherford et al., 1994) for the isomeric structure, SLe^x, in agreement with findings that these two molecules have very similar average conformations in solution. The Fucα1−4GlcNAc and Galβ1−3GlcNAc linkages are very restricted in their movement and can be desribed as rigid linkages, as shown previously (Mukhapadhyay & Bush 1991; Homans & Forster, 1992) for smaller oligosaccharide analogs. Also the Galβ1−4Glc linkage appears to be very restricted. However, the GlcNAcβ1−3Gal linkage fluctuates between two conformational states, in agreement with the two low-energy conformations found after simulated annealing for this linkage.

DISCUSSION

The common elements of the three oligosaccharides LNFPII, SuLNFPII, and SLNFPII are virtually identical in solution as determined by NMR spectroscopy and MD simulations, and thus it is clear that the charged groups have no effect on the average conformations. As in the short chain analogs, the Le^a domain at the non-reducing end approximates a rigid structure. The Gal−Glc domain at the reducing end is also rigid, but the two domains are joined by a linkage that is flexible and fluctuates mainly between two minimum energy structures. The different behavior for the GlcNAcβ1−3Gal linkage is in agreement with the larger coupling constant between GlcNAcH1 and Gal^{4}C3 when compared to the long-range ^{1}H,^{13}C coupling constants for the other H1−C1−O*x*−C*x* glycosidic linkages. The NeuAcα2−3Gal linkage is also flexible, as already documented for the short chain analogs, and fluctuates mainly between two minimum energy structures.

^{1}H−^{1}H distance restraints were obtained from 1D- and 2D-ROESY spectra. The 1D experiment proved to be of importance in elucidating contributions from overlapping protons. We performed a 2D single-quantum multiple-bond correlation, a selective ^{13}C proton-detected 1D experiment, and ^{1}H,^{13}C double-selective proton-detected 1D experiments in order to obtain long-range ^{1}H,^{13}C coupling constants across the glycosidic linkages. Thus, the selective 1D experiments—so far reported only for di- and trisaccharides (Poppe & van Halbeek, 1991a,b)—were applied to a hexasaccharide, SLNFPII, relying on the natural ^{13}C abundance.

A prerequisite for the successful application of these 1D experiments is that the proton and carbon atoms can be excited selectively. In the case of the hexasaccharide, SLNFPII, it is difficult to obtain information on the Galβ1−3GlcNAc linkage (see Results section) because of the considerable overlap in the carbon dimension. The suggested

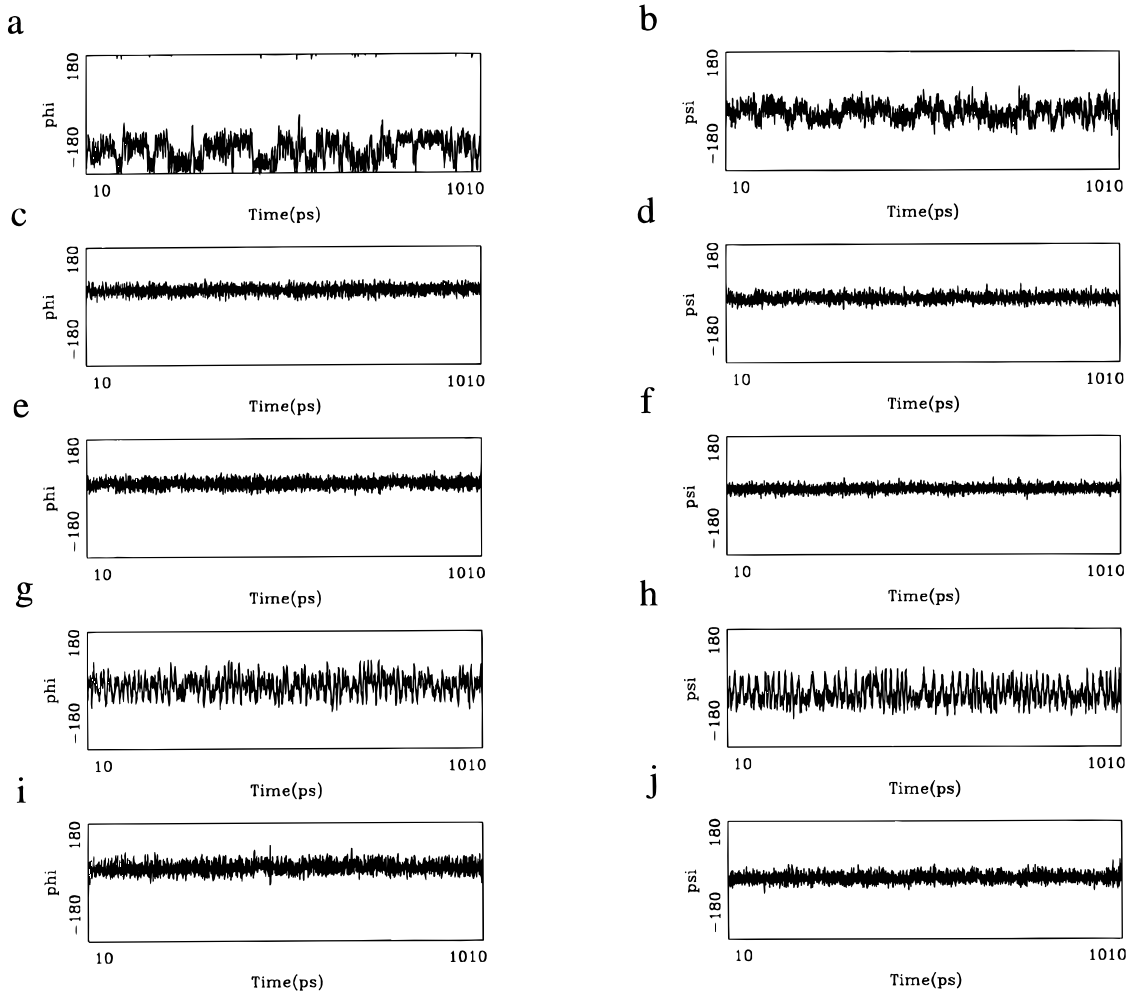

FIGURE 8: Trajectories from MD simulations of SLNFPII recorded at 300 K for 1 ns; (a) ϕ, time (ps) for Neuα2−3Gal; (b) ψ, time (ps) for NeuAcα2−3Gal; (c) ϕ, time (ps) for Galβ1−3GlcNAc; (d) ψ, time (ps) for Galβ1−3GlcNAc; (e) ϕ, time (ps) for Fucα1−4GlcNAc; (f) ψ, time (ps) for Fucα1−4GlcNAc; (g) ϕ, time (ps) for GlcNAcβ1−3Gal; (h) ψ, time (ps) for GlcNAcβ1−3Gal; (i) ϕ, time (ps) for Galβ1−4Glc; (j) ψ, time (ps) for Galβ1−4Glc. Data were extracted from MD runs after an initial equilibration period of 10 ps.

measurement by Poppe and van Halbeek (1991a) for obtaining coupling constants across the C1−O*x*−C*x*−H*x* glycosidic linkage by first applying a TOCSY step, would be considerably limited in the case of SLNFPII as a result of the severe chemical shift overlap in the carbon dimension.

For the NeuAcα2−3Gal linkage in SLNFPII, Gal^{3}H3 and NeuAcH3ax are in close proximity, as deduced from the intense ROE. We found a ROE between NeuAcH8 and Gal^3-H3ax, which was only barely above the noise level. The average ^{1}H−^{1}H distances derived from the simulations were in accord with these ROE's, thus establishing that the approximate distribution of conformers for the NeuAcα2−3Gal linkage is 65% conformers A and C and 35% conformer B (Figure 6).

It is interesting to note that the NeuAcα2−3Gal linkage in SLe^x, when bound to E-selectin, was reported (Cooke et al., 1994) to approximate to only one of the low-energy conformations (as in conformers A and C) for this linkage. This conclusion was based on a negative finding, namely, that no NOE could be detected between Gal^{3}H3 and NeuAcH3ax.

Studies of the bound conformations are required to explain the molecular basis for the greater binding strengths of the pentasaccharide-based ligands compared with the trisaccharide-based analogs. In order to establish the conformational distribution around the NeuAcα2−3Gal linkage in bound state using transferred NOE's it will be important to investigate whether the intensity for the NOE between Gal^3-H3 and NeuAcH8 increases upon binding. In a recent study (Scheffler et al., 1996) in which the conformation of SLe^x tetrasaccharide bound to E-selectin was investigated, a strong transferred NOE was indeed detected between these two protons, and thus the conformation around the NeuAcα2−3Gal linkage as depicted in conformers A and C could be established as the sole conformer in the bound state.

Our findings show, that the rigid Le^a-based domain at the non-reducing ends of the longer chain Le^a-type oligosaccharides, SuLNFPII and SLNFPII, may well approximate to fit as a lock and key model into a carbohydrate-binding site. We suggest that the flexibility of the linkage of the additional, rigid lactosyl domain at the reducing ends of the pentasaccharide-based ligands may be important for binding with little strain to extended carbohydrate-binding sites on the recognition proteins.

ACKNOWLEDGMENT

We thank Trevor Rutherford for having supplied us with the md-process program.

SUPPORTING INFORMATION AVAILABLE

The complete ^{1}H chemical shift assignments for SuLNFII and SLNFPII and the complete ^{13}C chemical shift assignments for LNFPII, SuLNFPII and SLNFPII are given (5 pages). Ordering information is given on any current masthead page.

REFERENCES

Ball, G. E., O'Neill, R. A., Schultz, J. E., Lowe, J. B., Weston, B. W., Nagy, J. O., Brown, E. G., Hobbs, C. J., and Bednarski, M. D. (1992) *J. Am. Chem. Soc. 114*, 5449−5451.

Bax, A., & Davies, D. G. (1985a) *J. Magn. Reson. 63*, 207−213.

Bax, A., & Davies, D. G. (1985b) *J. Magn. Reson. 65*, 355−360.

Bax, A., Griffey, R. H., & Hawkins, B. L. (1983a) *J. Am. Chem. Soc. 105*, 7188−7190.

Bax, A., Griffey, R. H., & Hawkins, B. L. (1983b) *J. Magn. Reson. 55*, 301−315.

Bechtel, B., Wand, A. J., Wroblewski, K., Koprowski, & Thurin, J. (1990) *J. Biol. Chem. 265*, 2028−2037.

Bendall, M. R., Pegg, D. T., & Doddrell, D. M. (1983) *J. Magn. Reson. 52*, 81−117.

Bevilacqua, M. P., & Nelson, R. M. (1993) *J. Clin. Invest. 91*, 379−387.

Bezouška, K., Yuen, C.-T., O'Brien, J., Childs, R. A., Chai, W., Lawson, A. M., Drbal, K., Fišerová, A., Pospíšıl, M., & Feizi, T. (1994) *Nature 372*, 150−157.

Bock, K., Brignole, A., & Sigurskjold, B. W. (1986) *J. Chem. Soc., Perkin Trans. 2*, 1711−1713.

Bock, K., & Duus, J. O. (1994) *J. Carbohydr. Chem. 13*, 513−543.

Breg, J., Kroon-Batenburg, L. M. J., Strecker, G., Montreuil, J., & Vliegenthart, J. F. G. (1989) *Eur. J. Biochem. 178*, 727−739.

Bush, C. A., & Cagas, P. (1992) *Adv. Biophys. Chem. 2*, 149−180.

Cagas, P., & Bush, C. A. (1990) *Biopolymers 30*, 1123−1138.

Cooke, R. M., Hale, R. S., Lister, S. G., Shah, G., & Weir, M. P. (1994) *Biochemistry 33*, 10591−10596.

Feizi, T. (1981) *TIBS 6*, 333−335.

Feizi, T. (1985) *Nature 314*, 53−57.

Feizi, T. (1993) *Curr. Opin. Struct. Biol. 3*, 701−710.

Feizi, T., & Childs, R. A. (1987) *Biochem. J. 245*, 1−11.

Giorda, R., Rudert, W. A., Vavassori, C., Chambers, W. H., Hiserodt, J. C., & Trucco, M. (1990) *Science 249*, 1298−1300.

Hakomori, S. (1985) *Cancer Res. 45*, 2405−2414.

Homans, S. W. (1990) *Biochemistry 29*, 9110−9118.

Homans, S. W., & Forster, M. J. (1992) *Glycobiology 2*, 143−151.

Ichikawa, Y., Lin, Y.-C., Dumas, D. P., Shen, G.-J., Garcia-Junceda, E., Williams, M. A., Bayer, R., Ketcham, C., Walker, L., Paulson, J. C., & Wong, C.-H. (1992) *J. Am. Chem. Soc. 114*, 9283−9298.

Kessler, H., Anders, V., Gemecker, B., & Steuernagel, S. (1989) *J. Magn. Reson. 85*, 1−14.

Kogelberg, H., & Rutherford, T. J. (1994) *Glycobiology 4*, 49−57.

Lin, Y. C., Hummel, C. W., Huang, D. H., Ichikawa, Y., Nicolaou, K. C., & Wong, C. H. (1992) *J. Am. Chem. Soc. 114*, 5452−5454.

Lubineau, A., Le Gallic, J., & Lemoine, R. (1995) *Bioorg. Med. Chem. 2*(11), 1143−1151.

Mukhapadhyay, C., & Bush, C. A. (1991) *Biopolymers 31*, 1737−1746.

Mukhapadhyay, C., Miller, K., & Bush, C. A. (1994) *Biopolymers 34*, 21−29.

Müller, L. (1979) *J. Am. Chem. Soc. 101*, 4481−4484.

Mulloy, B., Frenkiel, T. A., & Davies, D. B. (1988) *Carbohydr. Res. 184*, 39−46.

Neuhaus, D., Wagner, G., Vašák, N., Kägi, J. H. R., & Wüthrich, K. (1985) *Eur. J. Biochem.*, 151, 257−273.

Norwood, T. J., Boyd, J, Heritage, J. E., Soffe, N., & Campbell, I. D. (1990) *J. Magn. Reson. 87*, 488−501.

Poppe, L., & van Halbeek, H. (1991a) *J. Magn. Reson. 93*, 214−217.

Poppe, L., & van Halbeek, H. (1991b) *J. Magn. Reson. 92*, 636−641.

Poppe, L., & van Halbeek, H. (1992) *J. Magn. Reson. 96*, 185−190.

Rutherford, T. J., Spackman, D. G., Simpson, P. J., & Homans, S. W. (1994) *Glycobiology 4*, 59−68.

Scheffler, K., Ernst, B., Katopodis, A., Magnani, J. L., Wang, W. T., Weisemann, R., & Peters, T. (1995) *Angew. Chemie, Int. Ed. 34*, 1841−1844.

States, D. J., Haberkorn, R. A., & Ruben, D. J. (1982) *J. Magn. Reson. 48*, 286−292.

Yuen, C.-T., Lawson, A. M., Chai, W., Larkin, M., Stoll, M. S., Stuart, A. C., Sullivan, F. X., Ahren, T. J., & Feizi, T. (1992) *Biochem*istry *31*, 9126−9131.

Yuen, C.-T., Bezouška, K., O'Brien, J., Stoll, M., Lemoinne, R., Lubineau, A., Kiso, M., Hasegawa, A., Bockovich, N. J., Nicolaou, K. C., & Feizi, T. (1994) *J. Biol. Chem. 269*, 1595−1598.

BI9521598